JACS
JOURNAL OF THE AMERICAN CHEMICAL SOCIETY

ARTICLE

pubs.acs.org/JACS

Proton-Detected Solid-State NMR Reveals Intramembrane Polar Networks in a Seven-Helical Transmembrane Protein Proteorhodopsin

Meaghan E. Ward,[†] Lichi Shi,[†,§] Evelyn Lake,[†,∥] Sridevi Krishnamurthy,[‡] Howard Hutchins,[‡] Leonid S. Brown,[*,†] and Vladimir Ladizhansky[*,†]

[†]Department of Physics and Biophysics Interdepartmental Group, University of Guelph, Guelph, Ontario N1G 2W1, Canada

[‡]Bruker Biospin, Billerica, Massachusetts 01821, United States

Supporting Information

ABSTRACT: We used high-resolution proton-detected multidimensional NMR to study the solvent-exposed parts of a seven-helical integral membrane proton pump, proteorhodopsin (PR). PR samples were prepared by growing the apoprotein on fully deuterated medium and reintroducing protons to solvent-accessible sites through exchange with protonated buffer. This preparation leads to NMR spectra with proton resolution down to ca. 0.2 ppm at fast spinning (28 kHz) in a protein back-exchanged at a level of 40%. Novel three-dimensional proton-detected chemical shift correlation spectroscopy allowed for the identification and resonance assignment of the solvent-exposed parts of the protein. Most of the observed residues are located at the membrane interface, but there are notable exceptions, particularly in helix G, where most of the residues are susceptible to H/D exchange. This helix contains Schiff base-forming Lys231, and many conserved polar residues in the extracellular half, such as Asn220, Tyr223, Asn224, Asp227, and Asn230. We proposed earlier that high mobility of the F-G loop may transiently expose a hydrophilic cavity in the extracellular half of the protein, similar to the one found in xanthorhodopsin. Solvent accessibility of helix G is in line with this hypothesis, implying that such a cavity may be a part of the proton-conducting pathway lined by this helix.

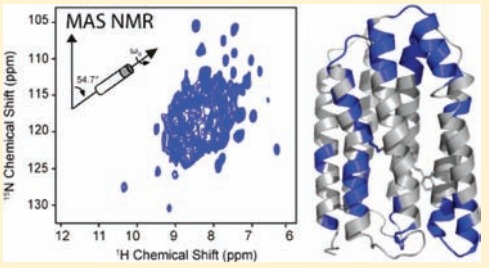

INTRODUCTION

Solid-state nuclear magnetic resonance (SSNMR) is quickly becoming a powerful tool for investigating the structure and function of membrane proteins in the lipid environment. Both magic angle spinning (MAS)[1,2] and oriented sample (OS) SSNMR experiments have produced unique structural and dynamic information.[3−11] Extensive amino acid assignments, the prerequisite for structural studies, have been obtained for several membrane proteins, and partial assignments have become available for many more.[12−18] These studies are currently complicated by comparatively poor sensitivity and insufficient spectral resolution due to the typically high molecular weight of membrane proteins, the high repetitiveness of hydrophobic residues, and the high degree of spectral overlap arising from the dominance of one type of secondary structure (i.e., from being mostly α-helical). One of the most promising ways to alleviate these problems is to employ detection of nuclei other than ^{13}C and ^{15}N, such as protons.

The high gyromagnetic ratio of protons makes these nuclei ideal for detection and has the potential to improve both the sensitivity and resolution of multidimensional SSNMR. Though MAS rates sufficient to resolve individual resonances are now obtainable,[19−22] smaller line widths can be obtained through the use of perdeuterated proteins with protons reintroduced at exchangeable sites. Proton-detected experiments on microcrystalline perdeuterated proteins have been shown to yield line widths rivaling those seen in solution NMR[23−26] and have recently been shown to yield sufficient resolution to resolve individual resonances in membrane and fibrillar proteins.[27] In this work we use proton-detected MAS SSNMR to study green proteorhodopsin (referred to as proteorhodopsin or PR in the following), a ubiquitous eubacterial light-driven seven-transmembrane (7TM) helical retinal-binding proton pump.[28] A high-resolution structure of PR has yet to be solved, as unlike its well-studied homologue bacteriorhodopsin (BR) it does not produce well-diffracting 3D crystals.[29] Most of the structural information on PR available so far has been derived from carbon and nitrogen chemical shifts determined by MAS SSNMR techniques.[16,17] To extend these studies to detect proton resonances, we have prepared a uniformly [^{13}C,^{15}N,^{2}H]-labeled sample of PR with protons reintroduced through back-exchange. As many studies have shown that the TM portions of membrane-anchored[30] and multispanning α-helical proteins are not susceptible to hydrogen−deuterium exchange[31−37] without employing additional unfolding-refolding protocols,[38] our sample is

Received: July 29, 2011
Published: September 16, 2011

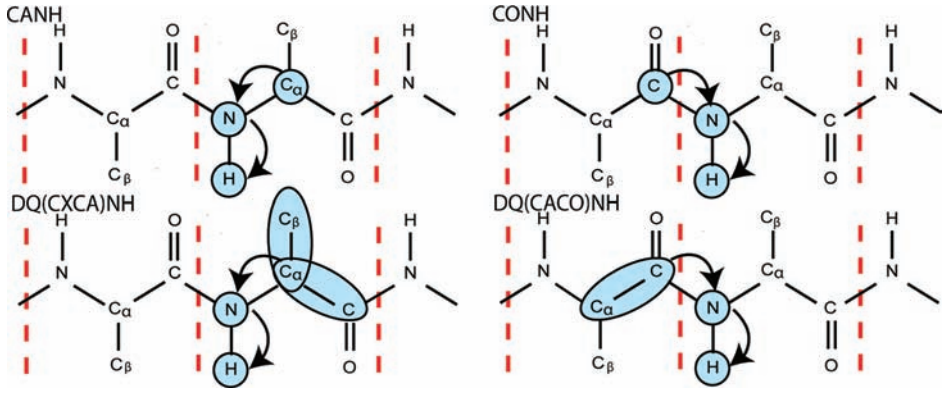

Figure 1. Assignment strategy. Systems are built by matching the $^{1}H-^{15}N$ frequencies of the CANH, CONH, DQ(CXCA)NH, and DQ(CACO)NH spectra and linking the ^{13}C information together. The CA[*i*] and CO[*i*-1] frequencies are obtained directly from the CANH and the CONH experiments, respectively, while the CO[*i*], CB[*i*], and CA[*i*-1] shifts are calculated from the information obtained from the DQ(CXCA)NH and DQ(CACO)NH combined with the information already gathered from the CANH and CONH experiments, respectively.

expected to contain protons only at exchangeable positions in solvent-accessible regions. In addition to loops, turns, and termini, these regions may include residues participating in proton conduction within the TM region of PR. In other proteins such regions can include functionally important hydrophilic cavities and channels which conduct ions and other polar substrates. Thus, in addition to providing higher sensitivity and an extra dimension for chemical shift dispersion in multidimensional experiments, the knowledge of the chemical shifts of solvent-accessible exchangeable sites will pave the way to directly observing functionally important groups.

The first step toward this goal is to obtain assignments of proton resonances. Our approach is based on a set of four dipolar-based three-dimensional (3D) chemical shift correlation experiments. As exchangeable protons are for the most part located only at the amide positions of the protein backbone, the polarization transfer pathways in perdeuterated proteins are limited by inefficient excitation of side chain carbons and necessity to transfer polarization back to amide protons for detection, as well as by the large spectral width of the carbon dimension. Through the use of dipolar-based INADEQUATE-type spectroscopy[39] for $^{13}C-^{13}C$ mixing and 3D proton detection experiments, it is possible to obtain sufficient information for sequential assignments of protein backbone resonances. In addition to serving as a basis for more detailed studies of PR function, the pattern of assigned residues provides information on the potential presence of a hydrophilic cavity in the TM region of the protein.

EXPERIMENTAL SECTION

Materials. Common chemicals of reagent grade were purchased from either Fisher Scientific (Unionville, Ontario, Canada) or Sigma-Aldrich (Oakville, Ontario, Canada). The isotopically labeled compounds such as $^{15}NH_4Cl$, $^{2}H,^{13}C_6$-glucose, ^{2}H-glucose, and deuterium oxide were obtained from Cambridge Isotope Laboratories (Andover, MA). The Ni^{2+}-NTA (nitrilotriacetic acid) agarose resin was purchased from Qiagen (Mississauga, Ontario, Canada). Lipids were purchased from Avanti Polar Lipids (Alabaster, AL).

Expression, Purification, and Reconstitution of PR. In the following, [U-$^{15}N,^{2}H$]-, [U-$^{13}C,^{15}N,^{2}H$]-, and [U-$^{13}C,^{15}N$]-labeled PR samples are referred to as UND, UCND, and UCN, respectively. UND and UCND samples were produced by optimizing a previously described protocol[16,17] for expression in 100% D_2O. Briefly, BL21-Codonplus-RIL *Escherichia coli* cells were transformed with a plasmid encoding C-terminally 6× His-tagged PR and cultured in 100% D_2O M9 minimal medium at 30 °C, using 4 g of either uniformly $^{2}H,^{13}C_6$-labeled or ^{2}H-labeled glucose, and 1 g of ^{15}N-labeled ammonium chloride per liter of culture as the sole carbon and nitrogen sources. As it was found that the cells could not survive at low densities in a 100% D_2O environment, the cells were grown to a high cell density in 2 mL and then 25 mL volumes before being added to the 1 L of culture to create a target cell density of A_{600} = 0.1 OD. These growth steps took approximately 24 and 15 h, respectively. The cells were then grown for ~6 h to reach a target cell density of A_{600} = 0.4 OD, at which point the expression of PR was induced by the addition of IPTG to a concentration of 1 mM. Protonated retinal was added exogenously at this time and twice after at intervals of ~7 h to a final concentration of 7.5 μM. After ~21 h the cells were collected by centrifugation and then treated with lysozyme (12 mg/L of culture) and DNase I (600 units/L culture) before being broken by sonication. The membrane fraction was then solubilized in 1% Triton X-100 at 4 °C in a regular H_2O-based buffer and purified using the same protocol described previously for the UCN sample.[16,17] A total of 15 mg of PR was purified from 1 L of culture. The molar amount of PR was determined by the absorbance of opsin-bound retinal, using the extinction coefficient of 44 000 M^{-1} cm^{-1}.[40]

The protein was reconstituted into liposomes composed of 1,2-dimyristoyl-*sn*-glycero-3-phosphocholine and 1,2-dimyristoyl-*sn*-glycero-3-phosphate mixed at a 9:1 ratio (w/w) at a protein:lipid ratio of 2:1 (w/w). The detergent-solubilized protein was mixed with the liposomes and incubated for 1 h at room temperature before Bio-Beads SM (Bio-Rad Laboratories) were added for detergent removal.

To achieve the desired level of proton back-exchange, proteoliposomes were incubated in a partially deuterated buffer for ~24 h and collected by ultracentrifugation at 150000*g* for 1 h. Reconstituted protein samples were packed into either a 2.5 or a 3.2 mm NMR rotor. We found that proton concentration at the exchangeable sites was higher than in the buffer. To rule out the possibility of residual protonation of our samples or that the protein experiences a higher back-exchange level at the purification stage, we recorded two types of control experiments. First, solution NMR $^{15}N-^{1}H$ HSQC TROSY spectra of the protein solubilized in detergent in 100% D_2O were recorded and showed no signal, ruling out the possibility of residual protonation. Second, a different sample preparation procedure was tested, in which 100% D_2O was used in the buffer at all stages, and back-exchange was performed after reconstitution. The 2D MAS $^{15}N-^{1}H$ correlation spectra and the proton concentration at the exchangeable sites did not

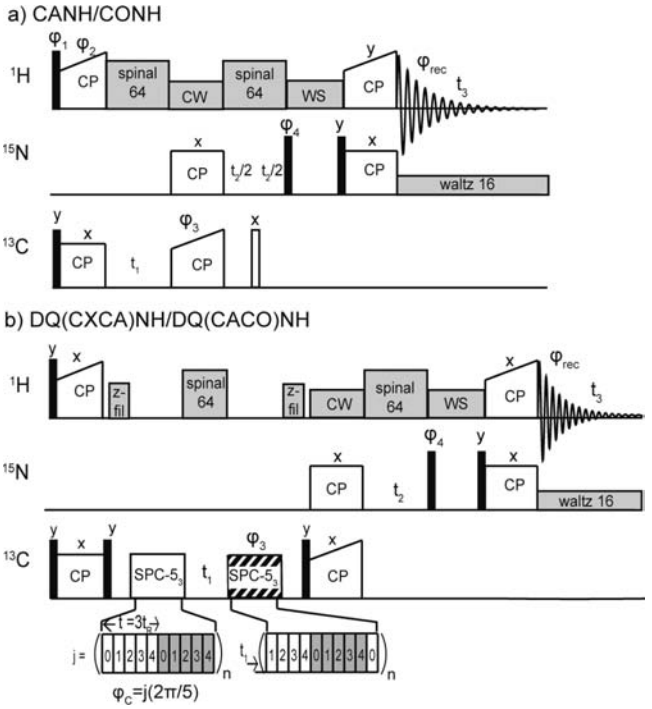

Figure 2. Pulse sequences for (a) CANH and CONH and (b) DQ-(CXCA)NH and DQ(CACO)NH experiments. Filled and hollow bars represent $\pi/2$ and π pulses, respectively. Both the CANH and DQ-(CXCA)NH experiments are identical to the CONH and DQ-(CACO)NH experiments, respectively, except for the position of the ^{13}C carrier frequency, which is set on CA for the CANH and CO for the CONH and is shifted to these values for the ^{13}C−^{15}N cross-polarization step in the corresponding DQ experiments. All experiments begin with a 90° pulse on both carbon and proton in order to increase initial polarization. During direct proton detection, ^{15}N-decoupling is performed using WALTZ-16.[54] The water suppression period was composed of a train of pulses applied at an rf field of 25 kHz and phase-shifted by $\pi/2$ every 12 ms for 240 ms. In panel a, the following phase cycling was used: $\varphi_1 = (y, y, -x, -x, -y, -y, x, x)$, $\varphi_2 = (x, x, y, y, -x, -x, -y, -y)$, $\varphi_3 = (x)$, $\varphi_4 = (y, -y)$, $\varphi_{rec} = (x, -x)$ and phase-sensitive detection is obtained in the indirect t_1 and t_2 dimensions by incrementing the phases φ_3 and φ_4, respectively, by 90°. In panel b the following phase cycle was used: $\varphi_3 = (x, y, -x, -y)$, $\varphi_4 = (y)$, $\varphi_{rec} = (-y, y, -y, y)$, and phase-sensitive detection is obtained in the indirect t_1 and t_2 dimensions by incrementing the phases φ_3 by 45° and φ_4 by 90°, respectively. To ensure rotor synchrony in the DQ(CXCA)NH experiment,[55,56] the reconversion block was further modified by incrementing the entire reconversion block by one C-element as shown in panel b, and by adding a phase shift of 144° to φ_C with every t_1 increment.

depend on whether D_2O or H_2O was used during the purification and reconstitution stages. Thus, it is likely that there are additional exchange effects with water in the air during sample packing. To minimize these effects, we put ~10 μL of buffer directly on top of the packed protein and then soaked the packed rotor in ~1 mL of buffer overnight at 4 °C. The rotor was then removed from the buffer and blotted dry before the spacer and the cap were reinserted. The samples stayed in the same buffer (inside the rotor) for extended periods of time (months), and no additional H/D exchange was observed. In the discussion below we refer to the effective proton concentration, which was assessed on the basis of the relative intensity of the ^{15}N spectrum and the intensity of the amide proton band of the proton spectrum. The functionality of the reconstituted protein has been tested using visible and FTIR spectroscopy as described previously.[16,17]

Assignment Strategy. The assignment strategy is based on four 3D chemical shift correlation proton-detected experiments (Figure 1). The dipolar-based CANH and CONH experiments, discussed in the following, provide CA[i]-N[i]-H[i] intra- and CO[i-1]-N[i]-H[i] inter-residue correlations, respectively. By comparing nitrogen and proton chemical shifts, these experiments can be matched to result in basic spin systems, CO[i-1]-N[i]-H[i]-CA[i]. To extend these systems into contiguous fragments, we make use of two additional experiments in which the N[i] and H[i] shifts are correlated to the DQ_{COCA} and DQ_{CACB} frequencies (DQ_{COCA} and DQ_{CACB} denote CO+CA and CA+CB double-quantum coherences (DQCs), respectively). The N[i] and H[i] shifts are correlated to the $DQ_{CACO}[i]$ and the $DQ_{CACB}[i]$ frequencies simultaneously in the DQ(CXCA)NH experiment (in which CX is CO or CB) and to the $DQ_{COCA}[i$-1] frequency in the DQ(CACO)NH experiment. These peaks are matched to result in $DQ_{COCA}[i$-1]-N[i]-H[i]-$DQ_{CACO}[i]$+$DQ_{CACB}[i]$ systems, which in turn can be compared to the CO[i-1]-N[i]-H[i]-CA[i] systems to calculate CA[i-1], CB[i], and CO[i] shifts and yield an extended CA[i-1]-CO[i-1]-N[i]-H[i]-CA[i]-CO[i]-CB[i] system. The resulting systems can then be linked through simultaneously matching the CO[i]/CO[j-1] and CA[i]/CA[j-1] shifts ($j = i$+1) between extended systems, whereas the amino acid type can often be determined using CB[i] shifts.

MAS SSNMR Spectroscopy. All NMR experiments were performed on a Bruker Biospin Avance III spectrometer operating at 800.230 MHz using either a 2.5 mm ^{1}H−^{13}C-^{15}N or a 3.2 mm ^{2}H−^{1}H-^{13}C−^{15}N probe set in triple resonance mode. Approximately 4 mg of UND PR was center-packed in a 2.5 mm rotor for an initial investigation of spectral quality as a function of spinning frequency and the level of back-exchange. Carbon−carbon correlation experiments and 3D chemical shift correlation spectroscopy were performed using a 3.2 mm probe. About 7 mg of UCND PR was center-packed in a 3.2 mm rotor. The effective temperature was kept at 5 °C in all experiments.

Typical $\pi/2$ pulses were 2.5 μs for ^{1}H, 5 μs for ^{13}C, and 7 μs for ^{15}N. The ^{1}H/X (where X is ^{15}N or ^{13}C) cross-polarization (CP)[41] contact times were 2 ms, with a constant radio frequency (rf) field of 35 and 50 kHz on nitrogen and carbon, respectively, while the proton lock field was ramped linearly around the n = 1 Hartmann−Hahn condition.[42] ^{13}CA/^{15}N and ^{13}CO/^{15}N band-selective transfers[43] were implemented with a contact time of 6 ms. For the ^{13}CA/^{15}N CP, a constant lock field of 2.5ν_r ($\nu_r = \omega_r/2\pi$, spinning frequency) strength was applied on ^{15}N, while the ^{13}C field was ramped linearly (5% ramp) around 1.5ν_r. For the ^{13}CO/^{15}N transfer, a constant lock field of 3.5ν_r field strength was applied on ^{13}C, while the ^{15}N field was ramped linearly (10% ramp) around 2.5ν_r. Optimized SPINAL64 decoupling[44] was used during indirect ^{15}N and ^{13}C chemical shift evolutions. The recycle delay was 2.5 s in all experiments.

Three-dimensional CANH and CONH chemical shift correlation experiments were recorded using the pulse sequence shown in Figure 2a. A total of 128, 96, and 1278 points were acquired in t_1, t_2, and t_3, leading to acquisition lengths of 6.4, 12.4, and 10.0 ms, respectively. Three-dimensional DQ(CXCA)NH and DQ(CACO)NH experiments were recorded using the pulse sequence shown in Figure 2b. For the DQ(CXCA)NH a total of 440, 68, and 1994 points were acquired in the in t_1, t_2, and t_3, leading to acquisition lengths of 6.4, 10.5, and 10.0 ms, respectively. For the DQ(CACO)NH a total of 260, 64, and 1994 points were acquired in t_1, t_2, and t_3, leading to acquisition lengths of 6.4, 9.9, and 10.0 ms, respectively. Each of the 3D experiments took about 3 days.

The excitation bandwidth of the Supercycled Post C-5 (SPC-5$_3$) sequence[45−47] at 20.5 kHz was sufficient to excite DQCs between CA and CB atoms, and this consideration dictated the choice of t_1 increment. In the DQ(CACO)NH experiment the DQ_{CACB} was not sampled because of the selectivity of the NCO CP transfer step. Thus, the t_1 increment was synchronized with one rotor cycle, States-TPPI[48] was used for phase-sensitive detection, and the resulting spectral width is

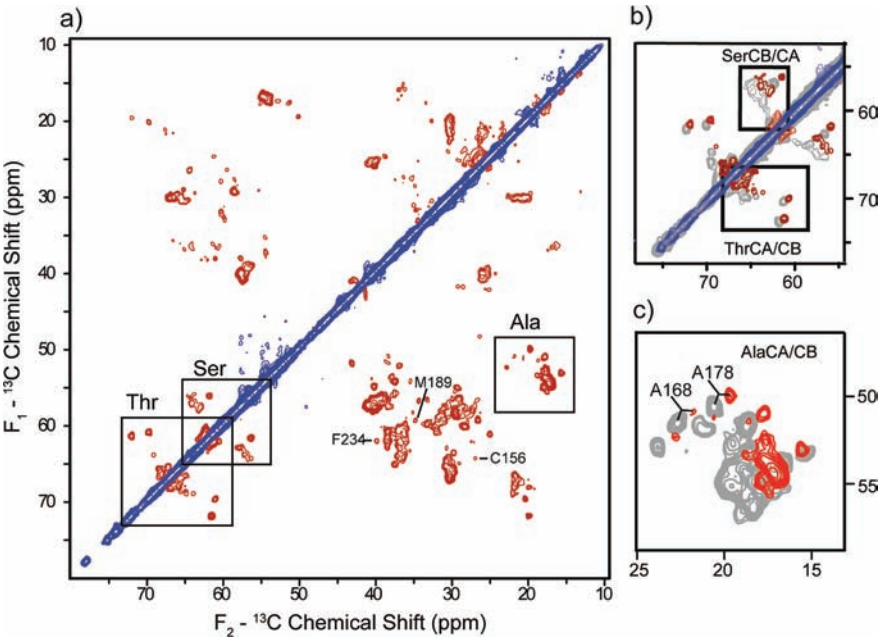

Figure 3. (a) 2D $^{13}C-^{13}C$ spectrum of UCND-labeled PR at 800 MHz proton frequency obtained with SPC-5_3 mixing. (b) Enlarged Thr and Ser Cα/Cβ region of the same spectrum. (c) Enlarged Ala Cα/Cβ regions. In panels b and c, the gray peaks shown are from the same experiment performed on an F,L,Y-reverse-labeled fully protonated sample.[16] Both data sets were processed identically using Lorentzian-to-Gaussian apodization in both dimensions.

Table 1. Summary of Chemical Shift Differences between UCN PR and UCND PR ($\Delta\delta(D) = \delta(D) - \delta(H)$)

residues	site	$\Delta\delta$(D) (ppm)
all	C′	0.3 ± 0.1
all	N	-0.3 ± 0.2
	CD	
Thr	Cα	-0.6 ± 0.1
Ala	Cα	-0.57 ± 0.08
Val, Ile	Cα	-0.71 ± 0.07
Asp, Asn, Phe, Tyr, Trp	Cα	-0.5 ± 0.2
Leu	Cα	-0.6 ± 0.1
Glu, Gln, Lys, Met	Cα	-0.6 ± 0.1
Thr	Cβ	-0.64 ± 0.09
Val	Cβ	-1.09 ± 0.02
	CD_2	
Gly	Cα	-0.60 ± 0.07
Asp, Asn, Phe, Tyr, Trp	Cβ	-0.9 ± 0.2
Glu, Gln, Met	Cβ	-1.1 ± 0.1
Leu	Cβ	-1.0 ± 0.1
	CD_3	
Ala	Cβ	-0.96 ± 0.05

fully sufficient to acquire the indirect DQ_{COCA} dimension without any spectral folding or aliasing. In the DQ(CXCA)NH experiment, both DQ_{CACO} and DQ_{CACB} are transferred through the NCA CP transfer step. To sample both types of coherences and avoid their spectral overlap, the carrier frequency was chosen at 112 ppm. Phase-sensitive detection of the t_1 indirect dimension was done using time-proportional phase incrementation (TPPI),[49] and the t_1 increment was set to the length of a single C-element of the SPC-5_3 block. Under these conditions the DQ_{COCA} state is sampled correctly in one half of the spectrum ranging from ~220 to 250 ppm, while the cross-peaks due to the DQ_{CACB} coherences are aliased into another empty half from ~150 to 210 ppm. Thus, both types of coherences do not overlap, and their frequencies can be extracted unambiguously. Further details of the phase cycle are given in the figure caption.

Data Processing and Analysis. Chemical shifts were referenced to DSS using the ^{13}C adamantane downfield peak resonating at 40.48 ppm as a secondary standard.[50] Data processing was performed using NMRPipe.[51] All 2D and 3D proton detected data were apodized with a sine-squared-bell function shifted by $\pi/3$ prior to taking the Fourier transform. Noise analysis, peak picking, and assignments were performed in the CARA[52] environment utilizing a suite of in-house-built LUA scripts and Autolink.[53]

RESULTS AND DISCUSSION

Spectral Resolution in Deuterated Samples. To evaluate how deuteration affects carbon spectral resolution and to assess water accessibility of various residues, we recorded a 2D $^{13}C-^{13}C$ correlation spectrum using SPC-5_3[45−47] as a mixing sequence. This spectrum, shown in Figure 3, exhibits a reduced number of peaks as compared to the UCN sample. Although water molecules are known to reside within the protein in a hydrogen-bonded network with polar amino acids in the retinal binding pocket,[57,58] many residues in the hydrophobic core are well protected from contacts with water by interhelical and protein−lipid hydrophobic interactions. They are not susceptible to the H/D back-exchange, do not contribute to the $^{1}H-^{13}C$ CP spectra, and do not show up in the 2D spectra. Apparent asymmetry of the spectrum is related to the nonuniform excitation of ^{13}C resonances, in which atoms more proximate to amide protons are excited to a higher degree. As a consequence, many cross peaks in the upper half of the spectrum (e.g., CB-CA, CG-CB) are weaker than their counterparts (CA-CB, CB-CG) in the lower half. One notable exception

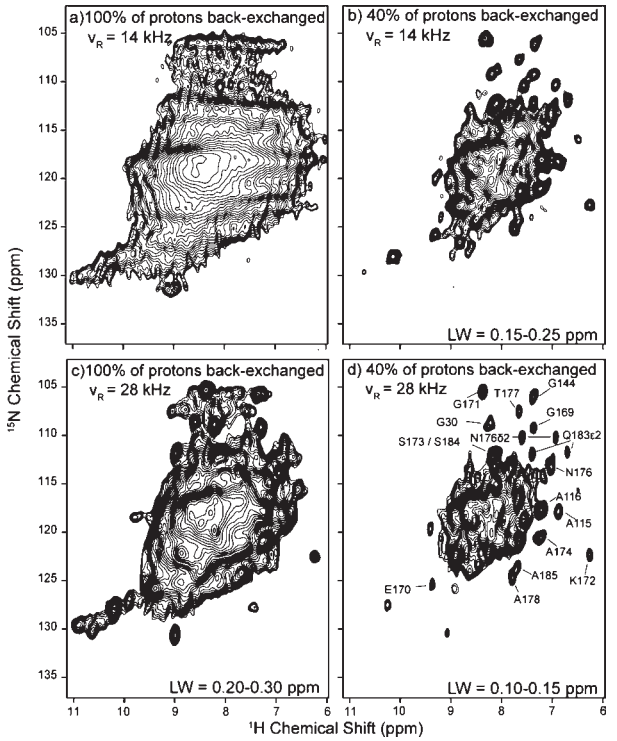

Figure 4. ^{1}H−^{15}N heteronuclear correlation spectra collected from a U-[^{2}H,^{15}N]-labeled sample of PR. Panels a and b were collected at a spinning frequency of 14 kHz, while c and d were collected at a spinning frequency of 28 kHz. For panels a and c the exchangeable sites were protonated at 100%, while for panels b and d the protonation level was 40%.

to this is observed for threonine and serine residues, whose side-chain CB atoms are likely excited by exchangeable hydroxyl protons and are of comparable intensity to the backbone carbons.

The line widths of individually resolved resonances in Figure 3 are on the order of 0.5−0.7 ppm and are very similar to those seen in the UCN sample.[16,17] Similarly, the line widths of ^{15}N resonances are on the order of 0.7 ppm (data not shown), similar to what has been determined in nondeuterated samples. We thus conclude that the presence of deuterium does not cause any significant line broadening of these nuclei, which is in agreement with previously reported observations in deuterated ubiquitin[59] and GB1.[60]

We observe that the presence of deuterium produces a significant isotope effect,[61] causing shifts in carbon and nitrogen resonances. Despite these shifts, many isolated peaks can be readily reassigned by simply comparing the 2D spectrum with that of the UCN sample. The upfield deuterium-induced chemical shift changes in PR are on the order of ∼0.5−1.0 ppm for Cα and Cβ spins, while CO resonances are shifted downfield by ∼0.3 ppm and HN resonances are shifted upfield by ∼0.3 ppm. Though shifts occasionally agree with those reported previously for GB1,[60] many are significantly larger, generally tending in these cases to agree with predicted shift values.[62] Table 1 summarizes the chemical shift differences induced by the isotope effect for various amino acid types and carbon atoms.

Most of the resolved residues in the 2D ^{13}C−^{13}C spectrum are located in the loop and interfacial regions of the protein, which are expected to be solvent exposed. The S/N ratios of peaks of exposed residues vary significantly. For example, A168 and A178

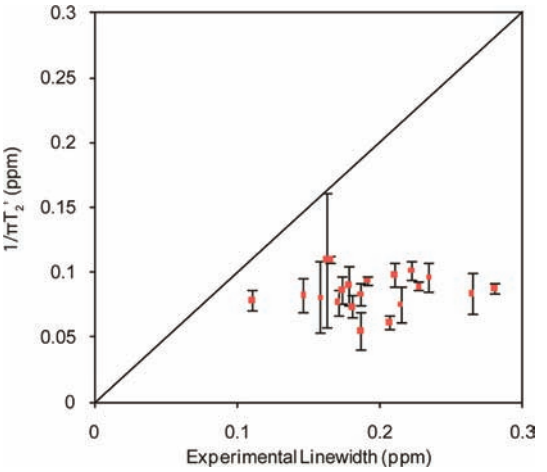

Figure 5. Comparison of predicted homogeneous line widths calculated from T_2' measurements to experimentally measured line widths (see Table S1 for identity of the atoms).

are both a part of the E-F loop, yet the intensity of the A168 peak relative to the A178 peak is greatly diminished in the UCND sample as compared to the UCN. Both alanines have Cα chemical shifts typical of a β-structure but very different backbone nitrogen shifts. While the A178 nitrogen chemical shift is 125.4 ppm (125.0 ppm in UCND) and consistent with a β-structure as predicted from the chemical shift index,[16,17] Ala168 has an anomalous chemical shift of 117.3 ppm (117.0 ppm in UCND), much lower than a typical alanine nitrogen shift.[63] We hypothesize that such a low chemical shift value is caused by a local electrostatic interaction, possibly with a negatively charged E165,[17] and this interaction may result in a low pK_a value for Ala168, short residence time of the amide proton and reduced intensity of Ala168 cross peaks.

We also detect residues that are predicted to be buried in the TM regions, e.g., C156, M189, and F234, which indicates that there are intramembrane portions of the protein that are accessible to water. Further evidence for water accessibility of specific TM regions of PR is discussed below.

Proton resolution shows a strong dependence on the proton concentration in the buffer and on the spinning frequency. Figure 4 compares 2D ^{1}H−^{15}N correlation spectra of a UND sample collected at different proton concentrations and spinning frequencies. The sample hydrated with 100% H_2O and spun at a moderate spinning rate, 14 kHz, gives spectra that lack any site-specific resolution. The resolution improves dramatically at faster spinning and/or lower proton concentrations. In a sample with exchangeable sites protonated at 40% and measured at 28 kHz spinning (Figure 4d), the line widths are in the range of 0.1−0.18 ppm, with many resolved peaks appearing in the spectrum. Overall, proton resolution is worse than that measured in microcrystalline SH3 or GB1 samples.[64,65] To further investigate the origin of the proton line width, a series of 2D ^{1}H−^{15}N spin−echo experiments were performed to estimate the residue-specific coherence lifetime (T_2') values.[66] Due to overlap in the 2D spectra, T_2' values were obtainable for only 22 residues. The values measured ranged from ∼3 to 6.5 ms, leading us to the conclusions that the homogeneous line widths predicted by the T_2' measurement were much smaller than the experimentally observed ones (Figure 5, Table S1) and that the residual line width is likely caused by structural heterogeneity.

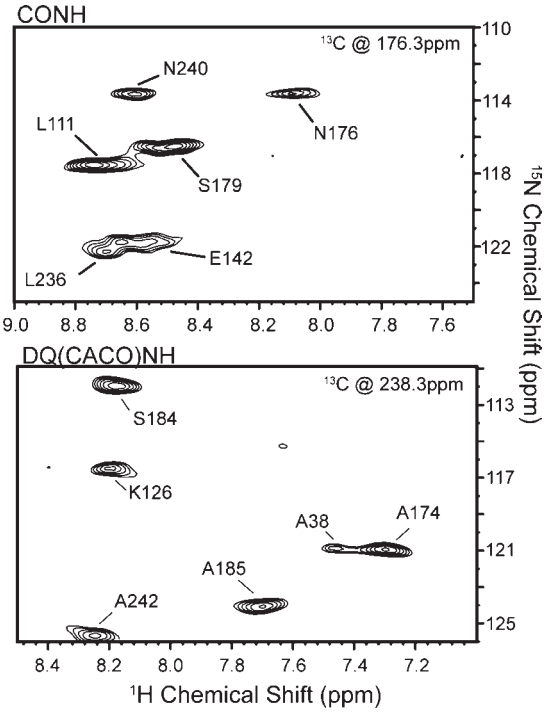

Figure 6. 2D planes of 3D CONH and DQ(CACO)NH experiments performed on UCND PR. All peaks are labeled according to the assignments. The first contour of each peak is cut at 4σ, with each additional level multiplied by 1.2.

Peak Picking and Assignment. Since spectral resolution was insufficient to resolve most peaks in the 2D experiments, 3D experiments were necessary to unambiguously assign resonances. As a compromise between sample volume and maximum achievable spinning frequency, a 3.2 mm rotor was used, and experiments were performed at a spinning frequency of 20.5 kHz to avoid rotational resonance conditions between CO and CA, and CO and CB resonances. Effective protonation at exchangeable sites was measured to be ~70%.

The assignment strategies were explained in the Experimental Section. Basic spin systems were built through matching CA[i]-N[i]-H[i] and CO[i-1]-N[i]-H[i] peaks of the CANH and COHN experiments, respectively. Approximately 100 of these systems were created, and they were found to vary significantly in their S/N ratios. Approximately half of the systems could be extended by the N[i]-H[i]-DQ$_{CACO}$[i] and N[i]-H[i]-DQ$_{COCA}$-[i-1] peaks. Representative 2D planes of the 3D experiments are shown in Figure 6. Fragments were built by simultaneously matching CO[i] and CA[i] shifts between the two extended systems, which was performed using Autolink[53] in the CARA[52] environment. Figure 7 shows an example of such a walk.

As mentioned previously, the SPC-5$_3$ sequence is sufficiently broadband to excite DQCs between CA and CB atoms. These DQCs can be detected in the DQ(CXCA)NH experiment and provide important information on the amino acid type through CB shifts, albeit the efficiency of DQ excitation for these types of coherences is generally lower. A total of 15 systems could be extended by adding the N[i]-H[i]-DQ$_{CACB}$[i] peaks, which allowed for the assignment of the amino acid type, or narrowing it down to fewer choices.

Through the identification of Gly, Ala, Ser, Thr, Val, and Ile residues and the categorization of the remaining residues, we were able to unambiguously assign 25 residues divided among three contiguous fragments (Figure 8). The fragment M140-M146 was identifiable by the unique G-X-X-G-I motif present from G141-I145. These assignments were strengthened by the amino acid type identification of A143 determined through CB data. The fragment G169-S179 was identified through the G-X-G-X pattern, which is unique to this segment. These assignments were strengthened by the amino acid type identifications of S173, A174, N176, and S179, which were determined through the CB data extracted from the DQ(CXCA)NH. The A181-N187 fragment was identified through the A-V-X-S pattern from A181-S184. These amino acid types were all determined using CA and CB shifts calculated from DQ(CXCA)NH data. Approximately 60 other systems were created and could not be assigned to the amino acid sequence due to insufficient information, such as a lack of CB data or an absence of the system in either or both of the DQ spectra. Many of these systems were, however, unambiguously identified through matching the available chemical shift information (CO[i-1]-N[i]-CA[i] or longer fragments) with those previously reported.[16,17] In addition, four side-chain resonances of Asn176 and Gln183 were identified in the CONH and DQ(CACO)NH spectra through matching the ^{15}N and ^{13}C shifts of these systems with those assigned previously.

Amino Acid Assignments and Structural Implications. Our findings are summarized in Figure 8, where we show an overall topology of PR with assigned exchangeable residues marked in blue, as well as its BR-based structural homology model. As expected, the majority of identified signals correspond to the surface residues, which directly interact with solvent. In particular, the cytoplasmic α-helical E-F loop and extracellular D-E loop are completely detectable and readily assignable in our experiments. Both loops give strong signals, suggesting that they have a more rigid structure than other loop regions. In contrast, only a few residues could be seen in the β-hairpin-forming B-C loop,[16] with their resonances being generally weaker. It is possible that strong hydrogen-bonding of some of the surface residues (such as those in the β-hairpin) precludes their H/D exchange.

From the NMR assignment pattern, it appears that, in PR, water molecules can typically penetrate to a depth of one or two helical turns into the intramembrane portion of the protein (Figure 8). Penetration depth appears to be larger on the cytoplasmic side. In particular, we observe strong signals from the cytoplasmic ends of helices C (Y110-A116), D (K126-V129), F (A181-N187), and G (F234-A242). Helices C, D, and F, along with the E-F helical loop, appear to form a localized cluster of exposed residues (Figure 8), which likely extends out of the lipid membrane into the cytoplasmic environment, forming a turret-like structure. Water penetration is generally shallower on the extracellular side. With the exception of helix G, we could see only tips of helices D (M140-E142) and E (W149-F152). Recent studies have shown that *Anabaena* sensory rhodopsin (ASR) is likely asymmetrically located in the bilayer, with the cytoplasmic side being more exposed to solvent,[18] and it appears that PR may have a similar position in the bilayer.

Interestingly, we detected several residues which are located in the TM parts of the protein, implying water accessibility of portions of the protein core. It should be noted that the H/D exchange may not correctly report on the solvent accessibility in every case, for example, when strong hydrogen bonds in the α-helices are present; on the contrary, dynamics of the helices may accelerate the exchange. Most notably, the backbone atoms from

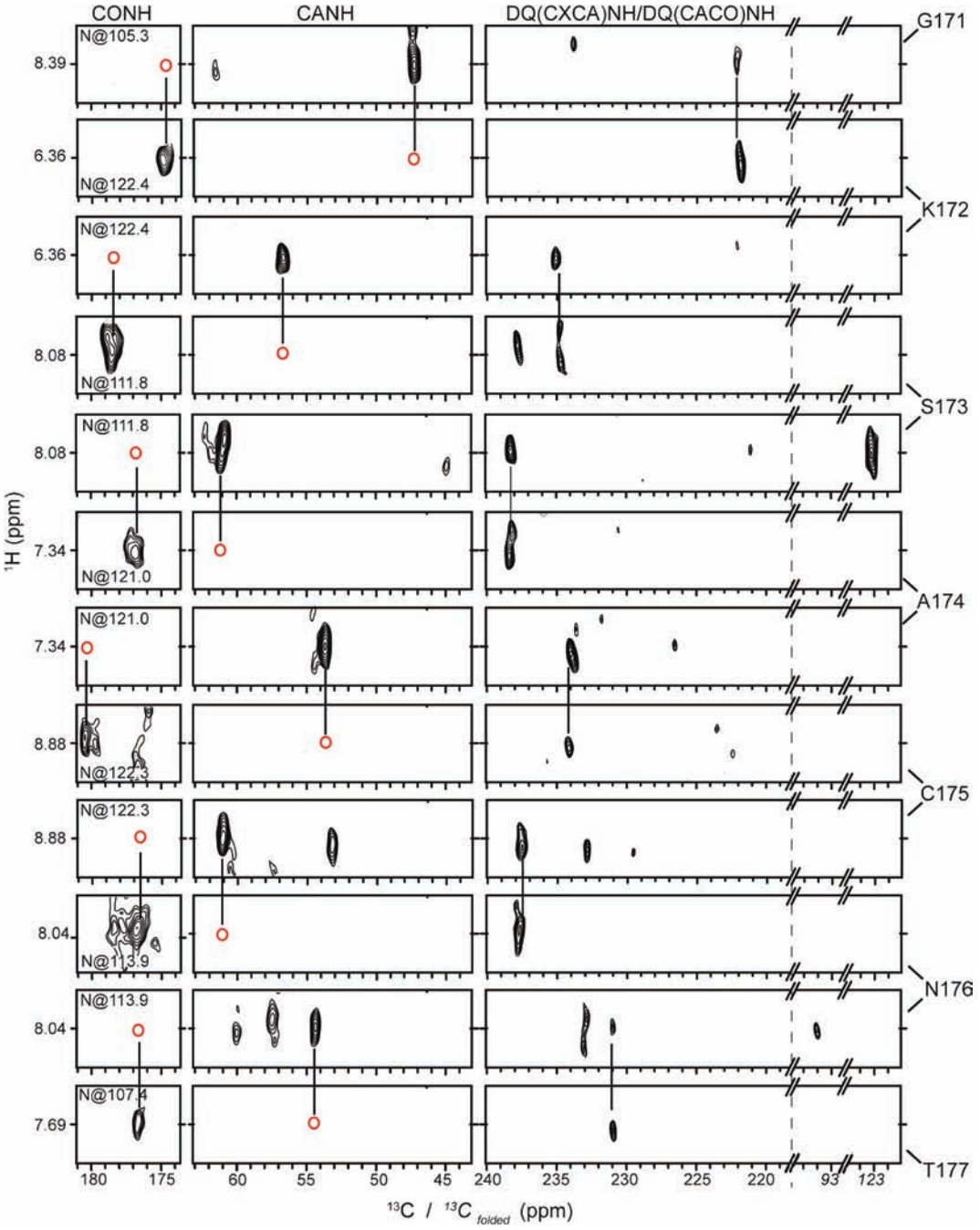

Figure 7. Sequential walk from G171 to T177 through the CANH, CONH, DQ(CXCA)NH, and DQ(CACO)NH spectra. Each strip is a ^{1}H−^{13}C 2D plane cut at the ^{15}N shift value indicated in each panel. The ^{1}H axis is always 0.5 ppm wide and centered on labeled shifts. A dashed line separates the DQ_{CACO} and DQ_{CACB} regions of the spectra. The axis on the DQ_{CACB} portion of the spectra is folded and thus runs in the opposite direction. Systems are linked together through matching the CA[*i*-1] and CO[*i*-1] of the *i*th system to the CA[*i*] and the CO[*i*] of the (*i*-1)th system. CA[*i*] and CO[*i*-1] values are detected directly in the CANH and CONH experiments. The CA[*i*-1] and the CO[*i*] values are calculated from the DQ_{COCA}[*i*-1] and DQ_{CACO}[*i*] frequencies detected in the DQ(CACO)NH and DQ(CXCA)NH experiments, respectively, and from the known CA[*i*] and CO[*i*-1] shifts. These calculated peaks are shown as red circles. CB[*i*] shifts can be calculated from the DQ_{CACB}[*i*] shifts detected in the DQ(CXCA)NH experiment and from the CA[*i*] shifts, and they also help identify many amino acid types and construct a backbone walk.

a large number of residues from helix G have been detected. A network of water-accessible residues within the TM region of helix G extends from the retinal Schiff base-forming Lys231 to the extracellular interface and includes polar residues such as Asn220, Tyr223, Asn224, Asp227, and Asn230, many of which are unique and conserved within the PR family[67] (e.g., N224, N230). They are spaced with the periodicity of an α-helix and likely form a hydrophilic face on the interior side of helix G. This hydrophilic face may be lining the proton-conducting pathway of PR.

Whereas proteorhodopsin and bacteriorhodopsin share some similarities in the initial stages of proton transport, i.e., retinal

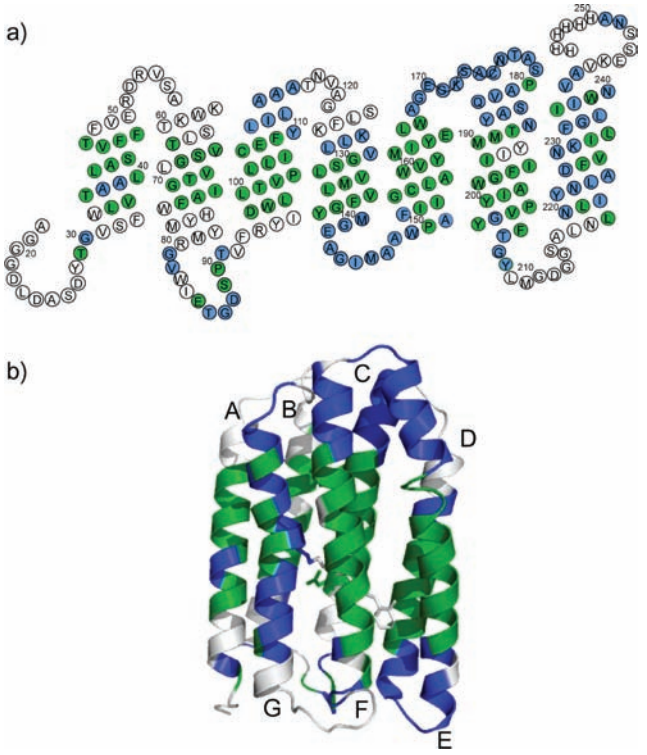

Figure 8. (a) Topological representation of PR with cytoplasmic side on top. All filled circles (blue or green) represent assigned residues. Blue circles represent residues with backbone atoms exposed to solvent. (b) 3D model of PR based on homology modeling using the 3D-JIGSAW[68] program and using the BR structure (PDB ID: 1C3W) as a template. Colors are as in panel a, and helices are labeled by letters. Helices A, B, C, and D are behind helices E, F, and G.

photoisomerization and deprotonation of the Schiff base, the proton release steps may be very different. While BR has a proton-releasing E194-E204 glutamate pair (in complex with water) located at the extracellular side of the protein, PR lacks homologous polar residues. We hypothesized previously that PR may contain a hydrophilic cavity on its extracellular side, similar to another homologous protein, xanthorhodopsin (XR),[69] and that access to this cavity may be modulated by conformational changes in the F-G loop.[17] The hydrophilic face of helix G can be connected to this cavity, forming a H-bonded network, which could be a part of the proton release mechanism. Homology modeling predicts that in PR this cavity could include the polar residues Glu142 and Tyr223, both of which are seen to be solvent accessible in our experiments. Interestingly, homologues of these two residues in XR have their side chains H-bonded via a water molecule. Our earlier data showed that the side chain of Glu142 is protonated even at high pH;[16] thus, it is possible that this proton is stabilized by H-bonding and is used for proton release to the extracellular bulk. It was also shown that E142Q mutation produces 15 nm spectral shift in the visible absorption and suppresses conformational changes of the backbone in the late stages of the photocycle,[70] supporting our idea that Glu142 may play an important role in PR function.

FTIR studies have shown that a H-bonded network of water molecules exists within the TM region of PR.[57,58] The side chain of His75, a highly conserved residue within the PR family that is predicted to be close to the photoactive site and potentially important in the proton transfer,[71,72] is seen to be solvent exposed, as it is visible in the 1D ^{15}N and 2D $^{1}H-^{15}N$ correlation spectra of our UNCD sample (data not shown). As His75 is H-bonded to the primary proton acceptor of the Schiff base Asp97,[72] a residue known to be exchangeable as shown by FTIR,[73] at least under illumination, this result is not unexpected. Judging from the homology with XR, both His75 and Asp97 could be a part of the above-mentioned H-bonded network supported by the polar residues in helix G and connected to the cavity facing F-G loop. In fact, such a network in XR includes the homologues of Lys231, Asp227, Asp97, and His75, and terminates by the homologue of Asn220 (Gln229). Thus, it is feasible that the injection of the Schiff base proton into the similar network of PR, enriched by additional unique Asn residues, will result in the proton release on the extracellular side.

CONCLUSIONS

We have demonstrated the feasibility of proton-detected multidimensional experiments in a perdeuterated 7TM membrane protein proteorhodopsin with protons reintroduced at the exchangeable sites through back-exchange. Proton resolution in PR was worse than that previously observed in SH3, GB1, or BR,[27,64,65] with approximately equal contributions to the line widths from homogeneous and heterogeneous sources. Large heterogeneous contributions suggest the presence of structural heterogeneity, while dynamics and residual proton−proton interactions between fully protonated retinal and amide protons of the protein may be responsible for the additional homogeneous line broadening. Even with the resolution available, the majority of resonances can be resolved site-specifically in 3D chemical shift correlation experiments and used to study solvent-accessible residues. Amide proton resonances were site-specifically assigned in 74 PR residues, most of which are located in the loop and termini regions of the protein, yet some residues in the protein core were found to be solvent accessible as well. In particular, the majority of the residues of transmembrane helix G were found to be H/D exchangeable, suggesting that this helix lines the proton-conducting pathway.

ASSOCIATED CONTENT

Supporting Information. Table of experimental line widths and theoretical homogeneous line widths calculated from site-specific coherence lifetime T_2' measurements. This material is available free of charge via the Internet at http://pubs.acs.org. The assigned chemical shifts have been deposited to BioMagResBank as BMRB entry 17817.

AUTHOR INFORMATION

Corresponding Author
lebrown@uoguelph.ca; vladizha@uoguelph.ca

Present Addresses
[§]Department of Medical Genetics & Microbiology, Medical Sciences Building, University of Toronto, Toronto, Ontario M5S 1A8, Canada
[∥]Department of Medical Biophysics, Sunnybrook Research Institute, Toronto, Ontario M4N 3M5, Canada

■ ACKNOWLEDGMENT

We thank Dr. M. Fey for technical support and assistance with optimizing the 3.2 mm HCN probe performance. This work was supported by Natural Science and Engineering Research Council of Canada, the Canada Foundation for Innovation, and the Ontario Ministry of Research and Innovation grants. V.L. holds Canada Research Chair Tier II in Biophysics. M.W. was supported by an NSERC Graduate Scholarship and by the Ontario Graduate Scholarship program. L.S. was supported by MITACS fellowship and by Bruker Canada Ltd.

■ REFERENCES

(1) Andrew, E. R.; Bradbury, A.; Eades, R. G. *Nature* **1958**, *182*, 1659–1659.
(2) Lowe, I. J. *Phys. Rev. Lett. 2* **1959**, *7*, 285–287.
(3) Naito, A. *Solid State Nucl. Magn. Reson.* **2009**, *36*, 67–76.
(4) Page, R. C.; Li, C.; Hu, J.; Gao, F. P.; Cross, T. A. *Magn. Reson. Chem.* **2007**, *45*, S2–S11.
(5) Gong, X. M.; Franzin, C. M.; Thai, K.; Yu, J.; Marassi, F. M. *Methods Mol. Biol.* **2007**, *400*, 515–529.
(6) Park, S. H.; Das, B. B.; De Angelis, A. A.; Scrima, M.; Opella, S. J. *J. Phys. Chem. B* **2010**, *114*, 13995–14003.
(7) Baldus, M. *Curr. Opin. Struct. Biol.* **2006**, *16*, 618–623.
(8) Hong, M. *J. Phys. Chem. B* **2007**, *111*, 10340–10351.
(9) Ramamoorthy, A. *Solid State Nucl. Magn. Reson.* **2009**, *35*, 201–207.
(10) McDermott, A. *Annu. Rev. Biophys.* **2009**, *38*, 385–403.
(11) Renault, M.; Cukkemane, A.; Baldus, M. *Angew. Chem., Int. Ed.* **2010**, *49*, 8346–8357.
(12) Egorova-Zachernyuk, T. A.; Hollander, J.; Fraser, N.; Gast, P.; Hoff, A. J.; Cogdell, R.; de Groot, H. J.; Baldus, M. *J. Biomol. NMR* **2001**, *19*, 243–253.
(13) Gammeren, A. J.; Hulsbergen, F. B.; Hollander, J. G.; Groot, H. J. *J. Biomol. NMR* **2005**, *31*, 279–293.
(14) Etzkorn, M.; Martell, S.; Andronesi, O. C.; Seidel, K.; Engelhard, M.; Baldus, M. *Angew. Chem., Int. Ed.* **2007**, *46*, 459–462.
(15) Li, Y.; Berthold, D. A.; Gennis, R. B.; Rienstra, C. M. *Protein Sci.* **2008**, *17*, 199–204.
(16) Shi, L.; Ahmed, M. A.; Zhang, W.; Whited, G.; Brown, L. S.; Ladizhansky, V. *J. Mol. Biol.* **2009**, *386*, 1078–1093.
(17) Shi, L.; Lake, E. M.; Ahmed, M. A.; Brown, L. S.; Ladizhansky, V. *Biochim. Biophys. Acta* **2009**, *1788*, 2563–2574.
(18) Shi, L.; Kawamura, I.; Jung, K.-H.; Brown, L. S.; Ladizhansky, V. *Angew. Chem., Int. Ed.* **2011**, *50*, 1302–1305.
(19) Ishii, Y.; Tycko, R. *J. Magn. Reson.* **2000**, *142*, 199–204.
(20) Paulson, E. K.; Morcombe, C. R.; Gaponenko, V.; Dancheck, B.; Byrd, R. A.; Zilm, K. W. *J. Am. Chem. Soc.* **2003**, *125*, 15831–15836.
(21) Zhou, D. H.; Shah, G.; Cormos, M.; Mullen, C.; Sandoz, D.; Rienstra, C. M. *J. Am. Chem. Soc.* **2007**, *129*, 11791–11801.
(22) Bertini, I.; Emsley, L.; Lelli, M.; Luchinat, C.; Mao, J.; Pintacuda, G. *J. Am. Chem. Soc.* **2010**, *132*, 5558–5559.
(23) Agarwal, V.; Diehl, A.; Skrynnikov, N.; Reif, B. *J. Am. Chem. Soc.* **2006**, *128*, 12620–12621.
(24) Chevelkov, V.; Rehbein, K.; Diehl, A.; Reif, B. *Angew. Chem., Int. Ed.* **2006**, *45*, 3878–3881.
(25) Agarwal, V.; Reif, B. *J. Magn. Reson.* **2008**, *194*, 16–24.
(26) Asami, S.; Schmieder, P.; Reif, B. *J. Am. Chem. Soc.* **2010**, *132*, 15133–15135.
(27) Linser, R.; Dasari, M.; Hiller, M.; Higman, V.; Fink, U.; Lopez del Amo, J. M.; Markovic, S.; Handel, L.; Kessler, B.; Schmieder, P.; Oesterhelt, D.; Oschkinat, H.; Reif, B. *Angew. Chem., Int. Ed.* **2011**, *50*, 4508–4512.
(28) Beja, O.; Aravind, L.; Koonin, E. V.; Suzuki, M. T.; Hadd, A.; Nguyen, L. P.; Jovanovich, S. B.; Gates, C. M.; Feldman, R. A.; Spudich, J. L.; Spudich, E. N.; DeLong, E. F. *Science* **2000**, *289*, 1902–1906.
(29) Gourdon, P.; Alfredsson, A.; Pedersen, A.; Malmerberg, E.; Nyblom, M.; Widell, M.; Berntsson, R.; Pinhassi, J.; Braiman, M.; Hansson, Ö. *Protein Expr. Purif.* **2008**, *58*, 103–113.
(30) Durr, U. H.; Yamamoto, K.; Im, S. C.; Waskell, L.; Ramamoorthy, A. *J. Am. Chem. Soc.* **2007**, *129*, 6670–6671.
(31) Earnest, T. N.; Herzfeld, J.; Rothschild, K. J. *Biophys. J.* **1990**, *58*, 1539–1546.
(32) Schulman, B. A.; Redfiend, C.; Peng, Z.-Y.; Dobson, C. M.; Kim, P. S. *J. Mol. Biol.* **1995**, *253*, 651–657.
(33) Baenziger, J. E.; Methot, N. *J. Biol. Chem.* **1995**, *270*, 29129–29137.
(34) Sturgis, J.; Robert, B.; Goormaghtigh, E. *Biophys. J.* **1998**, *74*, 988–994.
(35) Pinheiro, T. J. T.; Cheng, H.; Seeholzer, S. H.; Roder, H. *J. Mol. Biol.* **2000**, *303*, 617–626.
(36) Halskau, O.; Froystein, N. A.; Muga, A.; Martinez, A. *J. Mol. Biol.* **2002**, *321*, 99–110.
(37) Vinchurkar, M. S.; Chen, K. H. C.; Yu, S. S. F.; Kuo, S. J.; Chiu, H. C.; Chien, S. H.; Chan, S. I. *Biochemistry* **2004**, *43*, 13283–13292.
(38) Oxenoid, K.; Kim, H. J.; Jacob, J.; Sonnichsen, F. D.; Sanders, C. R. *J. Am. Chem. Soc.* **2004**, *126*, 5048–5049.
(39) Bax, A.; Freeman, R.; Kempsell, S. P. *J. Am. Chem. Soc.* **1980**, *102*, 4849–4851.
(40) Friedrich, T.; Geibel, S.; Kalmbach, R.; Chizhov, I.; Ataka, K.; Heberle, J.; Engelhard, M.; Bamberg, E. *J. Mol. Biol.* **2002**, *321*, 821–838.
(41) Pines, A.; Gibby, M. G.; Waugh, J. S. *J. Chem. Phys.* **1973**, *59*, 569–590.
(42) Hartmann, S. R.; Hahn, E. L. *Phys. Rev.* **1962**, *128*, 2042–2053.
(43) Baldus, M.; Petkova, A. T.; Herzfeld, J.; Griffin, R. G. *Mol. Phys.* **1998**, *95*, 1197–1207.
(44) Fung, B. M.; Khitrin, A. K.; Ermolaev, K. *J. Magn. Reson.* **2000**, *142*, 97–101.
(45) Hohwy, M.; Rienstra, C. M.; Jaroniec, C. P.; Griffin, R. G. *J. Chem. Phys.* **1999**, *110*, 7983–7992.
(46) Hohwy, M.; Rienstra, C. M.; Griffin, R. G. *J. Chem. Phys.* **2002**, *117*, 4973–4987.
(47) Huang, K. Y.; Siemer, A. B.; McDermott, A. E. *J. Magn. Reson.* **2011**, *208*, 122–127.
(48) States, D. J.; Haberkorn, R. A.; Ruben, D. J. *J. Magn. Reson.* **1982**, *48*, 286–292.
(49) Bodenhausen, G.; Vold, R. L.; Vold, R. R. *J. Magn. Reson.* **1980**, *37*, 93–106.
(50) Morcombe, C. R.; Zilm, K. W. *J. Magn. Reson.* **2003**, *162*, 479–486.
(51) Delaglio, F.; Grzesiek, S.; Vuister, G. W.; Zhu, G.; Pfeifer, J.; Bax, A. *J. Biomol. NMR* **1995**, *6*, 277–293.
(52) *The Computer Aided Resonance Assignment Tutorial*, 1st ed.; Keller, R., Ed.; Goldau: Switzerland, 2004.
(53) Masse, J. E.; Keller, R. *J. Magn. Reson.* **2005**, *174*, 133–151.
(54) Shaka, A. J.; Keeler, J.; Freeman, R. *J. Magn. Reson.* **1983**, *53*, 313–340.
(55) Hong, M. *J. Magn. Reson.* **1999**, *136*, 86–91.
(56) Brinkmann, A.; Eden, M.; Levitt, M. H. *J. Chem. Phys.* **2000**, *112*, 8539–8554.
(57) Bergo, V.; Amsden, J. J.; Spudich, E. N.; Spudich, J. L.; Rothschild, K. J. *Biochemistry* **2004**, *43*, 9075.
(58) Ikeda, D.; Furutani, Y.; Kandori, H. *Biochemistry* **2007**, *46*, 5365–5373.
(59) Morcombe, C. R.; Gaponenko, V.; Byrd, R. A.; Zilm, K. W. *J. Am. Chem. Soc.* **2005**, *127*, 397–404.
(60) Tang, M.; Comellas, G.; Mueller, L. J.; Rienstra, C. M. *J. Biomol. NMR* **2010**, *48*, 103–111.
(61) Batiz-Hernandez, H.; Bernheim, R. *Prog. Nucl. Magn. Reson.* **1967**, *3*, 63.
(62) Venters, R. A.; Farmer, B. T., II; Fierke, C. A.; Spicer, L. D. *J. Mol. Biol.* **1996**, *264*, 1101–1116.
(63) Wang, Y.; Jardetzky, O. *Protein Sci.* **2002**, *11*, 852–861.

(64) Zhou, D. H.; Shea, J. J.; Nieuwkoop, A. J.; Franks, W. T.; Wylie, B. J.; Mullen, C.; Sandoz, D.; Rienstra, C. M. *Angew. Chem., Int. Ed.* **2007**, *46*, 8380–8383.
(65) Akbey, U.; Lange, S.; Franks, W. T.; Linser, R.; Rehbein, K.; Diehl, A.; van Rossum, B. J.; Reif, B.; Oschkinat, H. *J. Biomol. NMR* **2010**, *46*, 67–73.
(66) De Paepe, G.; Giraud, N.; Lesage, A.; Hodgkinson, P.; Bockmann, A.; Emsley, L. *J. Am. Chem. Soc.* **2003**, *125*, 13938–13939.
(67) Brown, L. S.; Jung, K.-H. *Photochem. Photobiol. Sci.* **2006**, *5*, 538.
(68) Bates, P. A.; Kelley, L. A.; MacCallum, R. M.; Sternberg, M. J. *Proteins* **2001**, *Suppl. 5*, 39–46.
(69) Luecke, H.; Schobert, B.; Stagno, J.; Imasheva, E. S.; Wang, J. M.; Balashov, S. P.; Lanyi, J. K. *Proc. Natl. Acad. Sci. U.S.A.* **2008**, *105*, 16561–16565.
(70) Kralj, J. M.; Bergo, V. B.; Amsden, J. J.; Spudich, E. N.; Spudich, J. L.; Rothschild, K. J. *Biochemistry* **2008**, *47*, 3447–3453.
(71) Bergo, V. B.; Sineshchekov, O. A.; Kralj, J. M.; Partha, R.; Spudich, E. N.; Rothschild, K. J.; Spudich, J. L. *J. Biol. Chem.* **2008**, *284*, 2836–2843.
(72) Hempelmann, F.; Hölper, S.; Verhoefen, M.-K.; Woerner, A. C.; Köhler, T.; Fiedler, S.-A.; Pfleger, N.; Wachtveitl, J.; Glaubitz, C. *J. Am. Chem. Soc.* **2011**, *133*, 4645–4654.
(73) Dioumaev, A. K.; Brown, L. S.; Shih, J.; Spudich, E. N.; Spudich, J. L.; Lanyi, J. K. *Biochemistry* **2002**, *41*, 5348–5358.